

Synchronized Magnetization Oscillations in F/N/F Nanopillars

Kiwamu KUDO*, Rie SATO and Koichi MIZUSHIMA

Corporate Research and Development Center, Toshiba Corporation, Kawasaki, 212-8582, Japan

Current-induced magnetization dynamics in a trilayer structure composed of two ferromagnetic free layers and a nonmagnetic spacer is examined. Both free layers are treated as a monodomain magnetic body with an uniform magnetization. The dynamics of the two magnetizations is modeled by modified Landau-Lifshitz-Gilbert equations with spin-transfer torque terms. By solving the equations simultaneously, we discuss their various solutions in detail. We show that there exists the synchronous motion of two magnetizations among the various solutions; the magnetizations are resonantly coupled via spin-transfer torques and perform precessional motions with the same period. The condition to excite the synchronous motion depends on the difference between the intrinsic frequencies of the two ferromagnetic free layers as well as the magnitude of current.

KEYWORDS: spin-transfer torque, current-induced magnetization dynamics, Landau-Lifshitz-Gilbert equation, synchronization, magnetization oscillations

1. Introduction

Current-induced magnetization excitations in magnetic nanopillars, predicted by Slonczewski¹ and Berger² in 1996, have been extensively studied. The basic structure of nanopillars is ferromagnetic/nonmagnetic/ferromagnetic (F/N/F) trilayer structure. It has been demonstrated experimentally that a spin-polarized dc current through a “free” ferromagnetic layer can reverse its magnetization.^{3–8} Moreover, recent experiments have shown that a coherent precession of the magnetization at GHz frequencies is induced by a spin-polarized current and that its frequency of precession depends on applied field and current density.^{9–11} These magnetization dynamics, current-induced magnetization switching (CIMS) and coherent precession, provides the possibility to utilize the spin-transfer phenomena for various applications, such as magnetic random access memory cells, nanometer-sized microwave generators, and so on.

Most experimental studies about CIMS and microwave generation have concerned an “asymmetric” trilayer consisting of a free thin ferromagnetic layer and a thick ferromagnetic layer with a fixed magnetization. Accordingly, many theoretical works also have concerned the asymmetric structure.^{12–17} By active experimental and theoretical studies for the past ten years, many properties of magnetization dynamics in the asymmetric structure have already been clarified. On the other hand, the magnetization dynamics in a “symmetric” structure where both ferromagnetic layers play the same role as free layers has received little attention. It is reported recently that precessional dynamics of the thick layer as well as the thin layer are excited by current in the usual asymmetric sample.¹⁸ Therefore, it is important to examine what kind of magnetization dynamics can be excited in the two-free-layers structures.

In this paper, we examine current-induced magnetization dynamics in the F1/N/F2 nanopillars where both F1 and F2 are ferromagnetic free layers and N is a nonmagnetic spacer as illustrated in Fig. 1. By the current passing through the trilayer, the magnetizations of F1 and F2, \mathbf{M}_1 and \mathbf{M}_2 , interact with each other via spin-

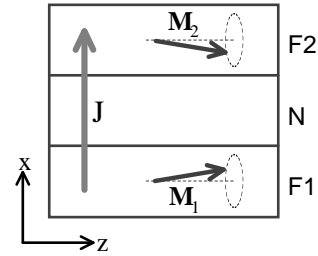


Fig. 1. Schematic of the F1/N/F2 trilayer. F1 and F2 are thin ferromagnetic “free” layers. N is a nonmagnetic spacer. J is current density perpendicular to plane. F1 and F2 are treated as a monodomain ferromagnet.

transfer torques,¹ and perform various motions. We discuss these motions in detail comparing with the magnetization dynamics in an asymmetric structure. We show that among these various motions there exists a synchronous motion of two magnetizations. In the motion, the two magnetizations perform a stable precessional motion with the same period, analogous to the synchronized oscillation of two coupled nonlinear oscillators. The synchronization of magnetizations may be efficient for raising the power of microwave radiation emitted by the magnetic multilayers which function as microwave generators.

2. Model

With regard to two ferromagnetic layers in the F1/N/F2 trilayer, we assume that both F1 and F2 have an uniaxial anisotropy in the z direction. We assume further that F1 and F2 have almost identical properties except that there is a difference between the magnitude of the effective magnetic fields acting on \mathbf{M}_1 and \mathbf{M}_2 . Within monodomain approximation, we describe the dynamics of the two magnetization vectors, \mathbf{M}_1 and \mathbf{M}_2 , by the modified Landau-Lifshitz-Gilbert equations

$$\frac{d\mathbf{m}_i}{d\tau} = -\mathbf{m}_i \times \mathbf{h}_{\text{eff}}^{(i)} + \alpha \mathbf{m}_i \times \frac{d\mathbf{m}_i}{d\tau} + \mathbf{\Gamma}_i, \quad (1)$$

with the spin-transfer torque term $\mathbf{\Gamma}_i$. Here we have used the dimensionless form of LLG equations. In eqs. (1), $\mathbf{m}_i = \mathbf{M}_i/M_s$, M_s is the saturation magnetization, times

*kiwamu.kudo@toshiba.co.jp

τ is measured in units of $(\gamma H_u^{(1)})^{-1}$, $H_u^{(1)}$ is the magnitude of the uniaxial anisotropy field acting on \mathbf{M}_1 , γ is the gyromagnetic ratio, and α is the dimensionless Gilbert damping constant of which we always take 0.01 in this paper. $\mathbf{h}_{\text{eff}}^{(i)}$ is the effective magnetic field normalized by $H_u^{(1)}$ and given by

$$\mathbf{h}_{\text{eff}}^{(i)} = (h_{\text{ext}}^{(i)} + h_u^{(i)} m_{iz}) \hat{\mathbf{z}} - h_p^{(i)} m_{ix} \hat{\mathbf{x}}, \quad (2)$$

where $h_{\text{ext}}^{(i)}$ is the external field applied along the z direction, $h_u^{(i)}$ is the in-plane uniaxial-anisotropy field ($h_u^{(1)} = 1.0$), and $h_p^{(i)} (\simeq 4\pi M_s / H_u^{(1)})$ is the effective out-of-plane anisotropy field due to the film shape of ferromagnets.

The spin-transfer torque term $\mathbf{\Gamma}_i$ acting on \mathbf{M}_i can be written in the form^{1,13}

$$\mathbf{\Gamma}_i = -a_J \mathbf{m}_i \times (\mathbf{m}_1 \times \mathbf{m}_2). \quad (3)$$

The parameter a_J represents the strength of the spin-transfer torque and is proportional to current density J . We assign the positive value of a_J for the current flowing from F1 to F2. It is noticed that the strength of the spin-transfer torque acting on \mathbf{m}_1 and \mathbf{m}_2 are equal because we have assumed that F1 and F2 have almost identical properties. By means of eqs. (3), the two magnetizations can interact with each other. The motion of \mathbf{m}_2 contributes to that of \mathbf{m}_1 via $\mathbf{\Gamma}_1$, and vice versa. Due to the form of eqs. (3), $\mathbf{\Gamma}_i = \mathbf{0}$ when \mathbf{m}_1 and \mathbf{m}_2 are parallel.

We solve eqs. (1) numerically and examine the current-induced dynamics of \mathbf{m}_i on the unit sphere $|\mathbf{m}_i| = 1$.¹⁹ We conduct the calculation using mainly the two parameter sets for the effective fields; (i) $h_{\text{ext}}^{(1)} = h_{\text{ext}}^{(2)} = 2.0$, $h_u^{(1)} = 1.0$, $h_u^{(2)} = 1.0 + \Delta h_u$, $h_p^{(1)} = h_p^{(2)} = 0.0$, and (ii) $h_{\text{ext}}^{(1)} = 1.0$, $h_{\text{ext}}^{(2)} = 1.0 + \Delta h_{\text{ext}}$, $h_u^{(1)} = h_u^{(2)} = 1.0$, $h_p^{(1)} = h_p^{(2)} = 10.0$. In the parameter set (i), we neglect the effect of out-of-plane demagnetizing fields $h_p^{(i)}$ for simplicity. On the other hand, the parameter set (ii) is realistic and experimentally realizable. In the both sets of parameters, we model the difference between the magnitude of effective magnetic fields acting on the two magnetizations by Δh_u and Δh_{ext} , respectively. We assume that $\Delta h_u \geq 0$ and $\Delta h_{\text{ext}} \geq 0$. Since $\Delta h_u \geq 0$ or $\Delta h_{\text{ext}} \geq 0$, we consider the trilayers where the magnitude of effective magnetic field acting on \mathbf{m}_2 is larger than that acting on \mathbf{m}_1 in both models (i) and (ii). As we discuss below, the difference of the effective magnetic fields, such as Δh_u and Δh_{ext} , has the essential role to arise a synchronous motion of the two magnetizations. By using the simpler model (i), we clarify the characteristics of the synchronous motion of the magnetizations. By using the model (ii), we show that the synchronous motion exists even in a realistic setup. The parameters in (ii) cover the essential features of magnetization dynamics in the almost symmetric F/N/F trilayers including the two free layers with $h_u^{(i)} \leq h_{\text{ext}}^{(i)} \ll h_p^{(i)}$. Note that $h_p^{(i)}$ is several tens of times larger than $h_u^{(i)}$ in usual film ferromagnets. Moreover, Δh_{ext} can be realized by a exchange-bias field as that in spin-valve pillars.

In both models (i) and (ii), the equilibrium direction of the two magnetizations along $\mathbf{h}_{\text{eff}}^{(i)}$ corresponds to $\mathbf{m}_i = \hat{\mathbf{z}}$ in the absence of current. Accordingly, it would be appropriate that $\mathbf{m}_i = \hat{\mathbf{z}}$ as the initial value at $\tau = 0$. However, when \mathbf{m}_1 and \mathbf{m}_2 are completely parallel at $\tau = 0$, the spin-transfer torque, eq. (3), does not work at all and any magnetization dynamics are not excited. Therefore, we permit that the two magnetizations shift slightly from their equilibrium directions and are initially not parallel each other. This is justified by taking into account the effect of finite temperature. In the real materials with temperature $T \neq 0$, thermal fluctuations always exist and then magnetizations fluctuate around their equilibrium points all the time. Therefore, we assume that two magnetizations are initially in the vicinity of their equilibrium points and are not parallel, although we do not take account of thermal fluctuations when we solve eqs. (1).

3. Synchronized Precession of Two Magnetizations

In this section, we discuss the synchronous motion of the magnetizations by showing the results of the calculation in model (i), i.e., $\alpha = 0.01$, $h_{\text{ext}}^{(1)} = h_{\text{ext}}^{(2)} = 2.0$, $h_u^{(1)} = 1.0$, $h_u^{(2)} = 1.0 + \Delta h_u$, $h_p^{(1)} = h_p^{(2)} = 0.0$. We consider only the case that the applied current is positive, $a_J > 0$, because the synchronization of two magnetizations do not occur when $a_J < 0$ in model (i).

3.1 Phase diagram

Depending on a_J and Δh_u , several distinct types of dynamical modes as the solutions of eqs. (1) are excited by the spin-transfer torque. Figure 2 shows the dependence of steady state solutions on a_J and Δh_u . In the region labeled S, the synchronized precession of two magnetizations on which we will focus in this section occurs. In the other regions which are labeled by P and W, any kind of coherent precessions do not exist. The region P denotes the region where a static parallel configuration of two magnetization occurs. The region W denotes the region where two magnetizations behave chaotic.

Figure 3 shows the typical behaviors of \mathbf{m}_1 and \mathbf{m}_2 in the region W. It is found that the behavior like magnetization switching arises irregularly. To obtain Fig. 3, we have used $m_{1z}(0) = 0.998$, $m_{2z}(0) = 0.999$, and $\varphi(0) = \pi/6$ as initial conditions. Here, $\varphi = \varphi_2 - \varphi_1$ where φ_i is the azimuthal angle of \mathbf{m}_i . In other words, φ is the angle between \mathbf{m}_1^\perp and \mathbf{m}_2^\perp which are the projections of \mathbf{m}_1 and \mathbf{m}_2 onto the xy -plane, respectively; see Fig. 5(d). In the horizontal axis of Fig. 3, f_0 is the intrinsic frequency of \mathbf{m}_1 in the absence of current. $f_0 = \omega_0 / 2\pi$, where ω_0 is given by the well-known formula,

$$\omega_0 = \sqrt{(h_{\text{ext}}^{(1)} + h_u^{(1)})(h_{\text{ext}}^{(1)} + h_u^{(1)} + h_p^{(1)})}. \quad (4)$$

ω_0 can be determined by the ferromagnetic resonance (FMR) experiment. We have introduced f_0 as the standard precessional frequency. In model (i), $f_0 = 3.0/2\pi$.

In the region S, both \mathbf{m}_1 and \mathbf{m}_2 precess around the z axis with circular forms. The circular trajectories of the precessional motion of \mathbf{m}_1 and \mathbf{m}_2 are shown in

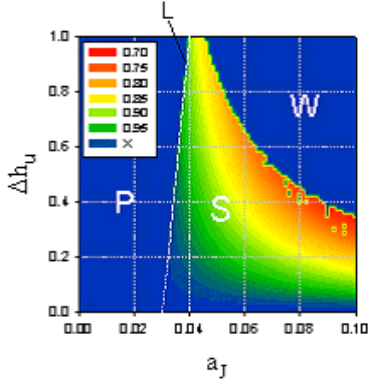


Fig. 2. (Color) Dynamical stability diagram for a_J and Δh_u . S denotes synchronized precession of two magnetization, P parallel configuration, and W chaotic motions. The numerical values in the legend represent the steady-state values of m_{1z} . X represents parallel configuration or chaotic motions. The broken line L represents the threshold for current-driven excitations.

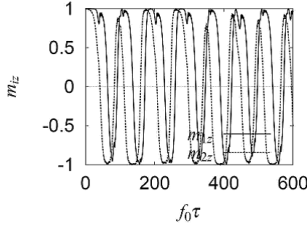


Fig. 3. Typical behaviors of \mathbf{m}_1 and \mathbf{m}_2 in the region W. Time evolution of $m_{iz}(\tau)$ is shown. The parameters are chosen as $a_J = 0.08$ and $\Delta h_u = 0.8$. The initial conditions are chosen as $m_{1z}(0) = 0.998$, $m_{2z}(0) = 0.999$, and $\varphi = \pi/6$.

Fig. 4(a). The steady precessions occurs after transient behaviors. The behaviors are shown in Fig. 4(b) where the time evolutions of $m_{1z}(\tau)$ and $m_{2z}(\tau)$ are plotted. Figure. 4(c) shows the time evolutions of the x components, $m_{1x}(\tau)$ and $m_{2x}(\tau)$, in the steady state at intervals between $f_0\tau = 300$ and 305 . As can be recognized from Fig. 4(c), the precessional frequencies of \mathbf{m}_1 and \mathbf{m}_2 are equal. In other words, the precessional phase is mutually locked. That is why we name the magnetization dynamics in the region S “synchronized precession” of two magnetizations.

3.2 Synchronized precessions

We discuss the properties of the synchronized precessions in detail.

The precessional amplitudes become large as a_J and Δh_u are increased. The dependence of the amplitude of \mathbf{m}_1 on a_J and Δh_u has been shown in Fig. 2. The legend in Fig. 2 represents the values of m_{1z} in the synchronized precessional state. Although it is not illustrated, the amplitude of \mathbf{m}_2 has the similar dependence on a_J and Δh_u as that of \mathbf{m}_1 . The difference between the precessional amplitude of \mathbf{m}_1 and \mathbf{m}_2 is that the amplitude of \mathbf{m}_2 is larger than that of \mathbf{m}_1 as is shown in Fig. 4(a) for any a_J and Δh_u . This property that $m_{1z} > m_{2z}$ is essential for the stability of the synchronous precession.

In the synchronized precession, the two magnetizations

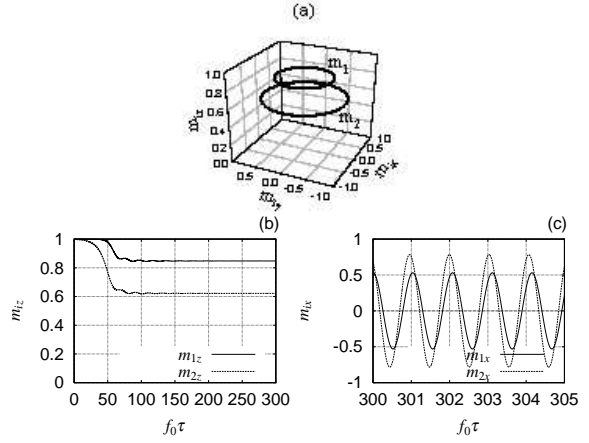


Fig. 4. Typical behaviors of \mathbf{m}_1 and \mathbf{m}_2 in the region S. The parameters are chosen as $a_J = 0.06$ and $\Delta h_u = 0.4$. The initial conditions are chosen as $m_{1z}(0) = 0.998$, $m_{2z}(0) = 0.999$, and $\varphi = \pi/6$. (a) Bird's-eye view of trajectories in the steady state. (b) Time evolution of $m_{iz}(\tau)$. (c) Time evolution of $m_{ix}(\tau)$ at intervals between $f_0\tau = 300$ and 305 .

precess around the z axis with the same period. Therefore, the phase shift φ is locked. The magnitude of the locking phase shift depends on a_J and Δh_u as is shown in Fig. 5(a). The numerical values in the legend of Fig. 5(a) represent the magnitude of φ/π . The phase shift becomes small as the magnitude of current increases.

The angle between \mathbf{m}_1 and \mathbf{m}_2 , $\phi = \arccos(\mathbf{m}_1 \cdot \mathbf{m}_2)$, also depends on a_J and Δh_u in the synchronized precessional state. The dependence is shown in Fig. 5(b). The numerical values in the legend of Fig. 5(b) represent the magnitude of ϕ/π . The angle between the two magnetization has the largest value in the precessional region where low a_J and high Δh_u .

The precessional frequency ω_s in the synchronized precession is tunable by current. In Fig. 5(c), we have shown the dependence of ω_s on a_J and Δh_u . The legend in the figure represents the value of ω_s . It is found that ω_s monotonously reduces as the magnitude of current increases.

Next, let us discuss the conditions for the excitation of the synchronized precession.

In Fig. 2, we have shown the threshold for the current-driven synchronized precession. The threshold is denoted by the broken line L. We have found that L can be estimated by $a_J = \alpha h_c^L$ where h_c^L is given by

$$h_c^L = h_{\text{ext}}^{(2)} + h_u^{(2)}. \quad (5)$$

Therefore, it is necessary that $a_J > \alpha h_c^L (= \alpha(3.0 + \Delta h_u))$ for the synchronized precession. It is noticed that the condition coincides with that for magnetization excitations in an asymmetric structure which can be obtained by a modified LLG equation; see eq. (17) in ref. 12. L corresponds to the threshold for magnetization excitations of \mathbf{m}_2 in a \mathbf{m}_1 -pinned asymmetric trilayers. The reason that the current threshold L depends on the effective magnetic fields acting on \mathbf{m}_2 can be understood as follows; when the two magnetizations, \mathbf{m}_1 and \mathbf{m}_2 , are initially almost parallel and a positive current ($a_J > 0$) is applied, the direction of the spin-transfer torque is such

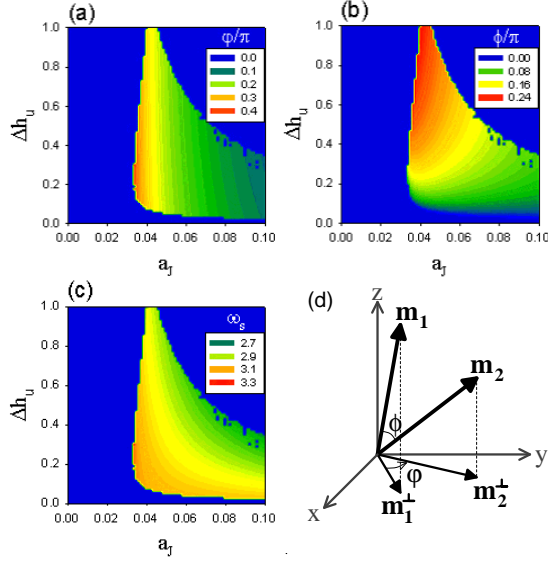


Fig. 5. (Color) (a) Dependence of the phase shift φ on a_J and Δh_u . (b) Dependence of the angle between the two magnetizations ϕ on a_J and Δh_u . (c) Dependence of the precessional frequency ω_s in the synchronized precession on a_J and Δh_u . (d) Definition of φ and ϕ .

that it induces the dynamics of \mathbf{m}_2 at first. On the other hand, when a negative current ($a_J < 0$) is applied, the direction of the spin-transfer torque is such that it induces the dynamics of \mathbf{m}_1 at first.

It is noticed that the region P has spread in all ranges of a_J for very small Δh_u in Fig. 2. Therefore, it is necessary that $\Delta h_u \neq 0$ as well as that $a_J > \alpha h_c^L$ for the excitation of the synchronized precession. In other words, it is necessary for the synchronized precession that the effective magnetic fields acting on the two magnetizations are different. We generalize this necessary condition in §4.3.

Finally, we compare the results discussed above with the ones obtained by the macrospin model in the asymmetric structures. In the modified LLG model for the asymmetric structures, coherent magnetization precessions are possible only when $h_u < h_{\text{ext}} < h_u + h_p$.¹⁷ Here h_{ext} , $h_u (= 1)$, and h_p are the dimensionless external magnetic field parallel to planes, in-plane uniaxial anisotropy field, and out-of-plane anisotropy field which act on the magnetization of the free layer, respectively. Accordingly, the out-of-plane anisotropy field h_p is important for current-induced magnetization precessions in the asymmetric structure. On the other hand, the synchronized magnetization precessions in the symmetric structure are possible even in the absence of $h_p^{(i)}$. Actually, we have neglected the effect of $h_p^{(i)}$ in this section.

4. Magnetization Dynamics in Realistic Trilayers

In this section, we discuss the magnetization dynamics including synchronized precessions in realistic trilayer structures. As a realistic setup, we use the set of parameters (ii): $\alpha = 0.01$, $h_{\text{ext}}^{(1)} = 1.0$, $h_{\text{ext}}^{(2)} = 1.0 + \Delta h_{\text{ext}}$, $h_u^{(1)} = h_u^{(2)} = 1.0$, and $h_p^{(1)} = h_p^{(2)} = 10.0$.

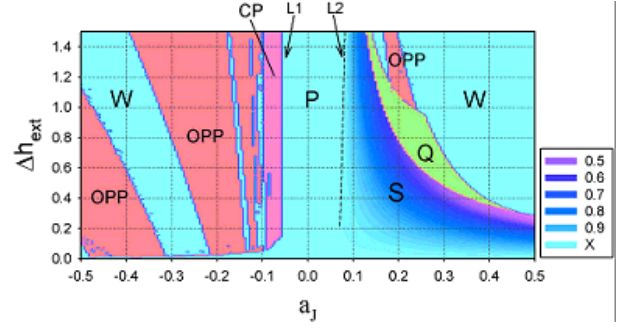


Fig. 6. (Color) Dynamical stability diagram for a_J and Δh_{ext} . S denotes synchronized precessions, Q quasi-periodic motions, OPP out-of-plane precessions, CP large-angle clamshell precessions, W chaotic behaviors, and P parallel configuration.²⁰ The numerical values in the legend represent the values of $\langle m_{1z} \rangle$. X represents parallel configuration or chaotic behaviors. The broken lines, L1 and L2, represent the threshold for current-driven excitations.

4.1 Phase diagram

In Fig. 6, the dynamical stability diagram for a_J and Δh_{ext} is shown. S, Q, OPP, CP, P, and W represent the region where synchronized precessions, quasi-periodic motions, out-of-plane precessions, clamshell precessions, parallel configuration, and chaotic behaviors occur, respectively. The numerical values in the legend represent the values of $\langle m_{1z} \rangle$ in the synchronized precession, where $\langle \dots \rangle$ is the one cycle average. The broken lines, L1 and L2, are the threshold for current-driven excitations. L1 and L2 can be estimated by $a_J = -\alpha h_c^{L1}$ where

$$h_c^{L1} = h_{\text{ext}}^{(1)} + h_u^{(1)} + \frac{h_p^{(1)}}{2} = 7.0, \quad (6)$$

and $a_J = \alpha h_c^{L2}$ where

$$h_c^{L2} = h_{\text{ext}}^{(2)} + h_u^{(2)} + \frac{h_p^{(2)}}{2} = 7.0 + \Delta h_{\text{ext}}, \quad (7)$$

respectively. It is then necessary that $a_J < -\alpha h_c^{L1}$ or $a_J > \alpha h_c^{L2}$ for magnetization excitations.

Let us first discuss the positive current region ($a_J > 0$) in Fig. 6.

In the region S, both \mathbf{m}_1 and \mathbf{m}_2 reach the steady precessional states after transient behaviors as shown in Fig. 7(a) and 7(b). In the steady state, the two magnetizations perform precessions around the z axis with elliptic forms, whose trajectories are shown in Fig. 7(c). The elliptic forms of the precessions result from the effect of the effective demagnetizing field $h_p^{(i)}$. As is shown in Fig. 7(d), the precessional period of \mathbf{m}_1 and \mathbf{m}_2 are identical. That is, the phase shift between \mathbf{m}_1 and \mathbf{m}_2 is locked. Therefore, the synchronized precessions exist even in a realistic setup. The precessional amplitudes become large as a_J and Δh_{ext} are increased. This tendency is the same as that discussed in the previous section.

For larger a_J or Δh_{ext} , the phase locking become weak and quasi-periodic motions occur. The region where the quasi-periodic motions occur is denoted as Q in Fig. 6. The typical motions of \mathbf{m}_1 and \mathbf{m}_2 in the region Q are shown in Fig. 8. Both \mathbf{m}_1 and \mathbf{m}_2 perform precessions around the z axis with several char-

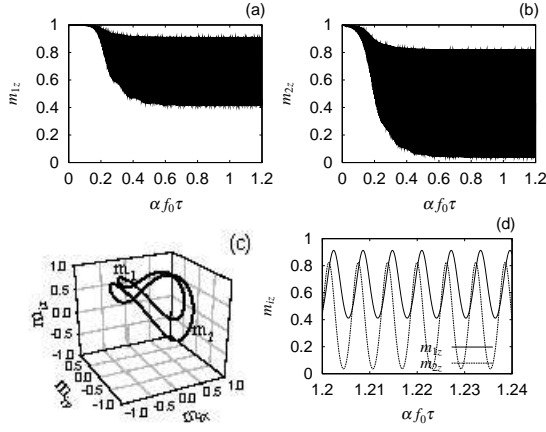


Fig. 7. Typical behaviors of \mathbf{m}_1 and \mathbf{m}_2 in the region S. The parameters are chosen as $a_J = 0.2$ and $\Delta h_{\text{ext}} = 0.6$. The initial conditions are chosen as $m_{1z}(0) = 0.999$, $m_{2z}(0) = 0.998$, and $\varphi = \pi/3$. (a) Time evolution of $m_{1z}(\tau)$. (b) Time evolution of $m_{2z}(\tau)$. (c) Bird's-eye view of the trajectories in the synchronized precession. (d) Time evolution of $m_{iz}(\tau)$ at intervals between $\alpha f_0 \tau = 1.2$ and 1.24 .

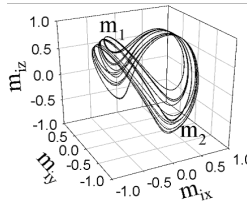


Fig. 8. Bird's-eye view of the trajectories in the region Q. The parameters are chosen as $a_J = 0.3$ and $\Delta h_{\text{ext}} = 0.6$.

acteristic frequencies. The typical power spectrum for the quasi-periodic motions is shown in Fig. 9(b). $I(\omega) \equiv \lim_{\tau \rightarrow \infty} \frac{1}{\tau} \langle m_{1x}^*(\omega) m_{1x}(\omega) \rangle$ is plotted, which is obtained by the Fourier transform of $m_{1x}(\tau)$ in the steady state. It is found that several characteristic frequencies coexist.

The phase boundary between the region S and Q is very sharp. In Fig. 9(a) and 9(b), we have shown the power spectrum for the steady-state motions at $(a_J, \Delta h_{\text{ext}}) = (0.24813, 0.6)$ and $(a_J, \Delta h_{\text{ext}}) = (0.24814, 0.6)$, respectively. It is determined by the very slight difference in a_J which motions will occur between synchronized precessions and quasi-periodic motions. The change to quasi-periodic motions from synchronized precessions is not continuous for a_J , i.e., the change is drastic.

In the region OPP, \mathbf{m}_2 performs the out-of-plane precession. On the other hand, \mathbf{m}_1 oscillates only around the vicinity of the positive z direction. Those behaviors are shown in Fig. 10(a). As a matter of fact, like the magnetization dynamics in the region S, \mathbf{m}_1 and \mathbf{m}_2 also perform precessions with the same period in the region OPP. However, because one of them has a small precessional amplitude, the magnetization dynamics of the whole system is almost an out-of-plane precession.

For too large a_J , chaotic behaviors of \mathbf{m}_1 and \mathbf{m}_2 occur. The typical behaviors are shown in Fig. 11(a) and 11(b) where time evolutions of $m_{1z}(\tau)$ and $m_{2z}(\tau)$ are plotted, respectively. \mathbf{m}_1 randomly changes its in-plane

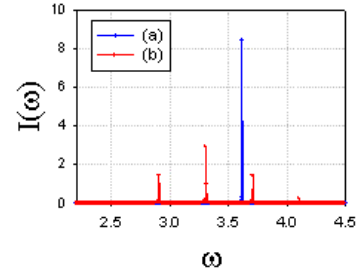


Fig. 9. (Color) (a) Typical power spectrum in the region S. The parameters are chosen as $(a_J, \Delta h_{\text{ext}}) = (0.24813, 0.6)$. (b) Typical power spectrum in the region Q. The parameters are chosen as $(a_J, \Delta h_{\text{ext}}) = (0.24814, 0.6)$.

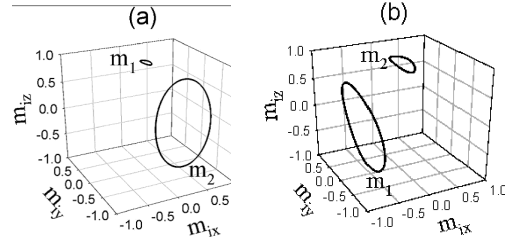


Fig. 10. Bird's-eye view of the trajectories in the region OPP. (a) Out-of-plane precession of \mathbf{m}_2 . The parameters are chosen as $a_J = 0.2 (> 0)$ and $\Delta h_{\text{ext}} = 1.2$. (b) Out-of-plane precession of \mathbf{m}_1 . The parameters are chosen as $a_J = -0.45 (< 0)$ and $\Delta h_{\text{ext}} = 0.6$.

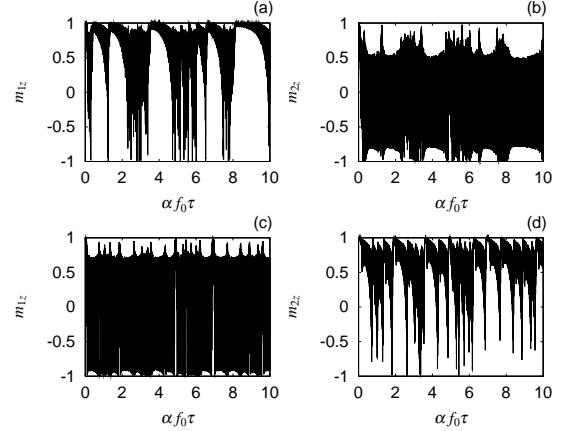


Fig. 11. Typical behaviors of $m_{iz}(\tau)$ in the region W. The initial conditions are chosen as $m_{1z}(0) = 0.999$, $m_{2z}(0) = 0.998$, and $\varphi = \pi/3$. (a)-(b) Typical behaviors in the region W where $a_J > 0$. The parameters are chosen as $a_J = 0.4$ and $\Delta h_{\text{ext}} = 0.6$. (c)-(d) Typical behaviors in the region W where $a_J < 0$. The parameters are chosen as $a_J = -0.35$ and $\Delta h_{\text{ext}} = 0.6$.

precessional amplitude. On the other hand, \mathbf{m}_2 hops between out-of-plane and in-plane trajectories irregularly.

Next, let us discuss the negative current region ($a_J < 0$) in Fig. 6.

In the region P, due to the smallness of current, any kind of magnetization dynamics is not excited. Just the static parallel configuration, $\mathbf{m}_1 = \mathbf{m}_2 = \hat{z}$, occurs in the steady state.

For the current exceeding the threshold L1, \mathbf{m}_1 performs an in-plane large-angle clamshell precession and,

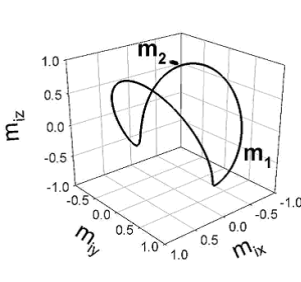


Fig. 12. Large-angle clamshell precession of \mathbf{m}_1 which occurs in the region CP. The parameters are chosen as $a_J = -0.085$ and $\Delta h_{\text{ext}} = 0.8$.

on the other hand, \mathbf{m}_2 moves only in the vicinity of the z axis. These typical behaviors are shown in Fig. 12. The behaviors become unstable at $a_J = -0.1$.

For $a_J < -0.1$, out-of-plane precessions of \mathbf{m}_1 or chaotic behaviors occur. In the region OPP, \mathbf{m}_1 performs the out-of-plane precession. On the other hand, \mathbf{m}_2 oscillates only around the vicinity of the positive z direction. Those behaviors are shown in Fig. 10(b). In the region W, chaotic behaviors of \mathbf{m}_1 and \mathbf{m}_2 occur. The typical behaviors are shown in Fig. 11(c) and 11(d) where time evolutions of $m_{1z}(\tau)$ and $m_{2z}(\tau)$ are plotted, respectively. \mathbf{m}_1 hops between out-of-plane and in-plane trajectory irregularly. \mathbf{m}_2 randomly changes its in-plane precessional amplitude. It is noted that according to the sign of current, the behavior of \mathbf{m}_1 and \mathbf{m}_2 is contrastive as can be recognized by comparing Fig. 10(a) with 10(b) and comparing Fig. 11(a)-(b) with 11(c)-(d). These behaviors in the region OPP and W reflect that the positive current region is the \mathbf{m}_2 -excited region and the negative current region the \mathbf{m}_1 -excited region.

In the negative current region ($a_J < 0$), the magnetization dynamics of the whole system is almost determined by \mathbf{m}_1 because \mathbf{m}_2 oscillates with very small amplitudes as mentioned above. Moreover, the obtained coherent behaviors in $a_J < 0$ are similar to those obtained by a macrospin model in an asymmetric structure: in-plane precessions and out-of-plane precession.⁹ Accordingly, roughly speaking, the magnetization dynamics is very similar to those in an asymmetric structure, especially its in-plane high magnetic field region; see Fig. 3 in ref. 9, for example. The difference is that there exists chaotic behaviors in our model.

4.2 Microwave frequency

Figure 13 shows the dependence of ω_1 on current a_J . ω_1 is the precessional frequency of \mathbf{m}_1 . Δh_{ext} is fixed as $\Delta h_{\text{ext}} = 0.6$. The dependence of ω_1 on a_J reflects the behaviors shown in Fig. 6 with $\Delta h_{\text{ext}} = 0.6$.

For the negative current regime ($a_J < 0$), we have obtained the dependence of microwave frequency on current similar to the one which can be obtained in the asymmetric structure.⁹ In the in-plane precessional region, the precessional frequency ω_1 decreases as the magnitude of current $|a_J|$ increases. In the out-of-plane precessional region, ω_1 increases as $|a_J|$ increases. ω_1 can not be defined in the region W because the characteristic frequency does

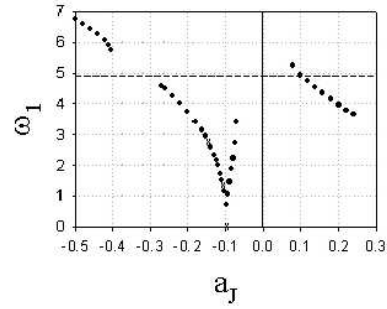


Fig. 13. Dependence of the precessional frequency ω_1 on a_J when $\Delta h_{\text{ext}} = 0.6$. The broken line represents $\omega_0 \simeq 4.9$ determined by eq. (4).

not exist in chaotic behaviors. Therefore, in Fig. 13, we have not plotted the data in the region W or have labeled several points by cross marks.

For the positive current regime ($a_J > 0$), we have plotted the dependence of ω_1 on a_J in the synchronized precession. The synchronized precessional frequency monotonously decreases as the magnitude of current is increased. This tendency is the same as that discussed in the previous section; see Fig. 5(c).

4.3 Conditions for the excitation of synchronized precessions

As can be found from Fig. 6, it is necessary that $\Delta h_{\text{ext}} \neq 0$ as well as $a_J > \alpha h_c^{L2}$ for the excitation of synchronized precessions. That is, the difference between the effective fields acting on two magnetizations is needed. This condition can be generalized; it is necessary that there exists the deviation between the intrinsic frequency of F1 and F2. The intrinsic frequency of \mathbf{m}_i is given by $\omega_0^{(i)} = \sqrt{(h_{\text{ext}}^{(i)} + h_u^{(i)})(h_{\text{ext}}^{(i)} + h_u^{(i)} + h_p^{(i)})}$. Accordingly, the above condition can be written as $\omega_0^{(1)} \neq \omega_0^{(2)}$. We have checked the condition using several sets of parameters. The condition that $\omega_0^{(1)} \neq \omega_0^{(2)}$ can be understood in the following way. If $\omega_0^{(1)} = \omega_0^{(2)}$, \mathbf{M}_1 and \mathbf{M}_2 tend to arrange their motions and become parallel to each other. As the result, the spin-transfer torque \mathbf{T}_i can not work. This condition is always applicable when \mathbf{M}_1 and \mathbf{M}_2 have their equilibrium points in the same direction in the absence of current.

It is noted that synchronized precessions can not exist when the deviation of intrinsic frequencies, $\Delta\omega = \omega_0^{(2)} - \omega_0^{(1)}$, is too large; $\Delta\omega \gg 0$. $\Delta\omega$ originates in the deviation of the effective magnetic fields such as Δh_u or Δh_{ext} . As it is recognized in Fig. 2 or 6, $\Delta\omega$ must be in a limited range, otherwise chaotic behaviors occur. One of the reason is that the phase locking of two magnetization precessions is impossible when $\Delta\omega$ is too large.

4.4 Comparison with macrospin models in an asymmetric structure

We compare the behaviors obtained by eqs. (1) with the ones obtained by the macrospin model in an asymmetric structure. It is known that two types of coherent magnetization motions of a free layer can be obtained

by an modified LLG equation in an asymmetric structure: in-plane precessions and out-of-plane precessions. Chaotic behaviors like telegraph noise can not be obtained by such an macrospin model because the degree of freedom of the magnetization is only two. Accordingly, the “W” phase experimentally observed by Kiselev *et al.*⁹ can not be obtained. In our model, however, chaotic behaviors can be obtained by eqs. (1) since the degree of freedom of the system is four. The region W appearing the negative current regime in Fig. 6 may corresponds to the “W” phase discussed in ref. 9.

5. Conclusions

Current-induced magnetization dynamics in a symmetric trilayer structure consisting of two ferromagnetic free layers and a nonmagnetic spacer is examined. We have treated the two free layers as a monodomain ferromagnet and calculated the magnetization dynamics by modified LLG equations. We have found that various behaviors of the two magnetizations arise depending on the applied current and the deviation of effective magnetic fields acting on them. Especially, there exists the synchronized precessions of two magnetizations among the various behaviors. For the excitation of the synchronization, current must exceed the threshold whose magnitude is the same as that for magnetization excitations in an asymmetric structure. It is also necessary that the intrinsic frequencies of the two magnetizations are different; $\omega_0^{(1)} \neq \omega_0^{(2)}$. Moreover, the deviation of frequencies, $\Delta\omega = \omega_0^{(2)} - \omega_0^{(1)}$, must be in a limited range for the phase locking of two magnetization precessions. Utilizing the synchronization in a symmetric trilayer may be one of the possible ways to raise the microwave emission power of the spin-transfer oscillators.^{21–23}

Acknowledgment

The authors would like to thank the staff of Frontier Research Laboratory in Toshiba Research & Development center for their daily help.

- 1) J. Slonczewski: J. Magn. & Magn. Mater. **159** (1996) L1.
- 2) L. Berger: Phys. Rev. B **54** (1996) 9359.
- 3) M. Tsoi, A. G. M. Jansen, J. Bass, W.-C. Chiang, M. Seck, V. Tsoi and P. Wyder: Phys. Rev. Lett. **80** (1998) 4281.
- 4) E. B. Myers, D. C. Ralph, J. A. Katine, R. N. Louie and R. A. Buhrman: Science **285** (1999) 867.
- 5) J. A. Katine, F. J. Albert, R. A. Buhrman, E. B. Myers: and D. C. Ralph, Phys. Rev. Lett. **84** (2000) 3149.
- 6) J. Grollier, V. Cros, A. Hamzic, J. M. George, H. Jaffres, A. Fert, G. Faini, J. Ben Youssef and H. Legall: Appl. Phys. Lett. **78** (2001) 3663.
- 7) J. Z. Sun, D. J. Monsma, D. W. Abraham, M. J. Rooks and R. H. Koch: Appl. Phys. Lett. **81** (2002) 2202.
- 8) S. Urazhdin, Norman O. Birge, W. P. Pratt, Jr. and J. Bass: Phys. Rev. Lett. **91** (2003) 146803.
- 9) S. I. Kiselev, J. C. Sankey, I. N. Krivorotov, N. C. Emley, R. J. Schoelkopf, R. A. Buhrman and D. C. Ralph: Nature **425** (2003) 380.
- 10) W. H. Rippard, M. R. Pufall, S. Kaka, S. E. Russek and T. J. Silva: Phys. Rev. Lett. **92** (2004) 027201.
- 11) I. N. Krivorotov, N. C. Emley, J. C. Sankey, S. I. Kiselev, D. C. Ralph and R. A. Buhrman: Science **307** (2005) 228.
- 12) J. Z. Sun: Phys. Rev. B **62** (2000) 570.
- 13) Z. Li and S. Zhang: Phys. Rev. B **68** (2003) 024404.
- 14) Ya. B. Bazaliy, B. A. Jones and Shou-Cheng Zhang: Phys. Rev. B **69** (2004) 094421.
- 15) G. Bertotti, C. Serpico, I. D. Mayergoyz, A. Magni, M. d'Aquino and R. Bonin: Phys. Rev. Lett. **94** (2005) 127206.
- 16) Jiang Xiao, A. Zangwill and M. D. Stiles: Phys. Rev. B **72**, (2005) 014446.
- 17) P. M. Gorley, P. P. Horley, V. K. Dugaev, J. Barnas and W. Dobrowolski: cond-mat/0508280.
- 18) S. I. Kiselev, J. C. Sankey, I. N. Krivorotov, N. C. Emley, A. G. F. Garcia, R. A. Buhrman and D. C. Ralph: Phys. Rev. B **72** (2005) 064430.
- 19) Since $\mathbf{m}_i \cdot \dot{\mathbf{m}}_i = 0$ from eqs. (1), it always holds that $|\mathbf{m}_i| = 1$.
- 20) The boundary between the region Q and OPP is very rough. At some points in Q near OPP, out-of-plane precessions also occur depending on initial conditions.
- 21) S. Kaka, M. R. Pufall, W. H. Rippard, T. J. Silva, S. E. Russek and J. A. Katine: Nature **437** (2005) 389.
- 22) F. B. Mancoff, N. D. Rizzo, B. N. Engel and S. Tehrani: Nature **437** (2005) 393.
- 23) J. Grollier, V. Gros and A. Fert: cond-mat/0509326.